Energy Storage Materials 27 (2020) 61–68

Contents lists available at ScienceDirect

Energy Storage Materials

journal homepage: www.elsevier.com/locate/ensm

High loading CuS-based cathodes for all-solid-state lithium sulfur batteries with enhanced volumetric capacity

Seyed Milad Hosseini [a,b], Alberto Varzi [a,b,**], Seitaro Ito [c], Yuichi Aihara [c], Stefano Passerini [a,b,*]

[a] Helmholtz Institute Ulm (HIU), Helmholtzstrasse 11, 89081, Ulm, Germany
[b] Karlsruhe Institute of Technology (KIT), P.O. Box 3640, 76021, Karlsruhe, Germany
[c] Samsung R&D Institute Japan, Senbanishi 2-1-11, Minoh, Osaka, Japan

ARTICLE INFO

Keywords:
Lithium
sulfur
Copper sulfide
Li/S–CuS
solid-state battery

ABSTRACT

Transition metal sulfides have shown to improve the performance of lithium-sulfur batteries both with liquid and solid electrolytes. In this work, the beneficial effect of copper sulfide for enabling high areal capacity lithium-sulfur all-solid-state batteries is shown. Copper sulfide-carbon (CuSC) and three different copper sulfide-sulfur-carbon (CuSS) composites are investigated as positive electrodes in all-solid-state lithium-sulfur batteries. The composites are prepared via facile and low-cost mechanochemical ball-milling. It is found that the CuS/C ratio greatly influences the redox properties of the CuSC cathode. Scanning electron microscopy, ex-situ X-ray diffraction, and galvanostatic cycling were also conducted to evaluate the CuSS composite electrodes in Li|LiI–Li_3PS_4|CuS–S–C solid-state cells. High mass loading cells made using these composite electrodes deliver capacities as high as 1600 mAh $g^{-1}_{(CuS+S)}$ and 7 mAh cm^{-2} at 20 °C. The higher density of CuS also leads to larger volumetric capacities, up to 3900 mAh $cm^{-3}_{(CuS+S)}$, thus enabling a potential energy density gain up to 15% with respect to a conventional Carbon–Sulfur cathode.

1. Introduction

All-solid-state lithium batteries have recently re-gained the attention of researchers due to the safety advantages of solid electrolytes (non-volatile and leak-less), that could enable the use of Li metal anodes without incurring into dendrite growth [1]. Additionally, compared with conventional liquid electrolytes, inorganic solid electrolytes offer higher transference number and, in some cases, wider electrochemical stability window, further boosting power and energy density of the resulting battery [2].

Despite these appealing premises and the effort of the scientific community, the successful transfer of research results from academic laboratories to commercial products is all but trivial. One of the biggest challenges is to achieve high areal capacities without penalizing the electrochemical performance of the cell. In fact, differently from liquid systems, point-to-point contacts are established between the active electrode material and the solid electrolyte, which considerably limit the active material utilization and require a large amount of solid electrolyte in the cathode. Electrode architectures with composition and morphology carefully designed to maximize ionic as well as electronic transport are therefore necessary.

Achieving high electrode loadings is particularly difficult for Sulfur-based cathodes, which notoriously suffer from sluggish kinetics due to the insulating nature of both S and Li_2S. Additionally, large volumetric changes up to 80% due to the lower density of Li_2S compared to elemental S need to be accounted for. Both these issues require the addition of large amounts of conductive additives, commonly carbon, in order to enable reversible conversion [3,4]. The introduction of large quantities of carbon further diminishes the already poor density of the Sulfur cathode, thus penalizing the volumetric energy density of the final Li–S cell.

A cathode with high areal capacity will also avoid large Li metal excess in the cell. While with conventional layered oxide cathodes the assembly of Li metal-free solid-state cells may be achievable, in Li–S cells the use of metallic lithium cannot be avoided. Currently, though, the manufacturing and handling of Li metal sheet thinner than 20 μm is extremely difficult [5]. This means that we need a cathode with, at least, 4.12 mAh cm^{-2} in order to fully balance the anode capacity. Although the importance of developing high loading S cathodes is recognized for liquid systems, it seems to be still neglected by the solid-state Li–S battery

* Corresponding author. Helmholtz Institute Ulm (HIU), Helmholtzstrasse 11, 89081, Ulm, Germany.
** Corresponding author. Helmholtz Institute Ulm (HIU), Helmholtzstrasse 11, 89081, Ulm, Germany.
E-mail addresses: alberto.varzi@kit.edu (A. Varzi), stefano.passerini@kit.edu (S. Passerini).

https://doi.org/10.1016/j.ensm.2020.01.022
Received 21 November 2019; Received in revised form 15 January 2020; Accepted 19 January 2020
Available online 22 January 2020

community. Indeed, although very appealing specific capacity values and cycle life have been demonstrated with various cathode configurations, so far the large majority of papers only reported data for electrodes with sulfur loading <1 mg cm^{-2} (see Table S.1), i.e., <1.6 mAh cm^{-2} (considering 100% S utilization) resulting on ca. 160% Li excess (for a 20 μm thick anode).

Previous works have demonstrated that transition metal sulfides (TMS) are electrode components/additives capable of enabling high areal capacity. In fact, they are known to improve the cell performance by increasing the electronic conductivity of the electrode, buffering the volume expansion, and contributing to increasing the electrode capacity by conversion reactions [6,7]. Several transition metal sulfides (TM_xS_y, TM = Co, Fe, Ti, Ni, etc.) have been investigated in the past few years, but mostly for liquid systems [8–13]. With regard, to solid-state systems, Yao et al. reported that the improved interface between cobalt sulfide and $Li_7P_3S_{11}$ solid electrolyte results in long cycling of the composite positive electrode [14]. Pyrite (FeS_2) was thoroughly investigated as cathode material, motivated by its highly appealing theoretical capacity (890 mAh g^{-1}), low cost, and high abundance [15–19]. In previous work, we have demonstrated the promising performance of pyrite-sulfur composite electrodes in all-solid-state lithium metal cells [20]. Interestingly, the crystalline structure of the composites is greatly influenced by the pyrite-sulfur ratio. The presence of pyrite in the thick composite electrode probably improves the electron percolation, enabling high areal capacity, 3.55 mAh cm^{-2} with 5 mg cm^{-2} active materials mass loading [20]. Following our previous work on iron disulfide, in this paper, we extend the study to copper sulfide (CuS). CuS, with its high electronic conductivity (up to 10^3 S cm^{-1}) and theoretical specific capacity (560 mAh g^{-1}) [21,22] is a very promising candidate, which was deeply investigated for primary batteries during the early stage of lithium batteries development [21,23–25]. Chung and Sohn studied copper sulfide as a cathode in conventional organic (liquid) electrolyte [21]. The proposed reaction mechanism involves two steps, the insertion of lithium in the copper sulfide lattice (at 2.05 V) followed by the conversion reaction to form metallic copper and lithium sulfide, occurring at 1.68 V. Unfortunately though, copper sulfide suffers from severe capacity fading in liquid electrolytes associated with the dissolution of copper at high potentials, as proved by Sun et al. [26] Later, Machida et al. and Hayashi et al. used elemental copper as an additive for sulfur electrodes in an all-solid-state cell featuring $60Li_2S–40SiS_2$ (mol %) as the electrolyte. The positive electrode was made via mechanical mixing of copper and sulfur, resulting in a composite of elemental sulfur, copper, $Cu_{1.8}S$ and CuS. The reaction mechanism proposed was in agreement with previous findings in liquid systems, with the additional contribution of sulfur at ca. 2.1 V upon lithiation, based on the reaction (1) [27,28].

$$S + 2Li^+ + 2e^- \rightarrow Li_2S \quad (1)$$

In either case, the delivered capacity was lower than the theoretical value and the cycling stability rather poor.

In this work, we deepen the electrochemical investigation of CuS in solid-state cells based on the sulfidic electrolyte (LiI–Li_3PS_4). First, we studied copper sulfide as positive electrode material with and without conductive additive (namely, CuS and CuSC(3–2)) to understand the reaction mechanism and the reasons behind the excellent long-term cycling performance of the material. Interestingly, it is found that copper sulfide partially reacts with the solid electrolyte already during the ball milling procedure used for preparing the composite electrode. Afterward, three CuS-sulfur-carbon composites with increasing sulfur content (namely CuSS(2–1), CuSS(1-1) and CuSS(1–2)) were prepared to probe the synergy between copper sulfide and sulfur. It is found that the formation of metallic copper upon discharge is crucial for achieving stable cycling. The CuSC(3–2) cathode with 1 $mg_{(CuS)}$ cm^{-2} mass loading delivers a specific capacity above 850 mAh g^{-1} for more than 800 cycles using lithium metal as an anode at 20 °C. Most interestingly, Copper sulfide-sulfur composite electrodes with high mass loading of 5 $mg_{(CuS+S)}$ cm^{-2} delivered high areal capacities up to 7 mAh cm^{-2} and potential energy density gain between 9 and 15% compared to pure S.

2. Results and discussion

Fig. 1a shows the XRD patterns of pristine (as obtained from supplier) CuS, ball-milled CuS (CuS-BM), and the CuSC(3–2) composite (see materials compositions in Table 1 and preparation details in the Methods section). It can be seen that the peak intensity of the ball-milled CuS is decreased compared to the pure CuS, suggesting that ball milling decreases the crystallite size [29]. The diffraction peak intensity is also lower in the CuS–C composite. In fact, the average crystalline domain size of the ball-milled samples is two times smaller than that of pure CuS (10 and 20 nm respectively), based on Scherrer equation (See Supp. Info). Nevertheless, the pure CuS structure (Covellite, ICDD PDF 03-065-0603, hexagonal, P63/mmc space group) is clearly retained in all samples. This demonstrates that no additional phase, such as, e.g., Cu_2S, is generated.

Scanning electron microscopy was used to study the morphology of these materials. The pristine CuS consists of micrometric particles with flower-like surface morphology (see Fig. 1b-c). Upon ball milling (CuS-BM), CuS break into sub-micrometric particles with more homogenous dispersion, which surface does not show the initial, characteristic morphology (see Fig. 1d-e). This supports the reduced XRD peaks intensity observed in Fig. 1a. The CuSC(3–2) mixture displays micrometric agglomerates, which are likely composed of the activated carbon particles, retaining their morphology, homogenously covered by copper sulfide sub-micrometric particles (see Fig. 1f-g) [20]. The Energy-dispersive X-ray spectroscopy (EDX) mapping of the CuSC(3–2) sample (see Fig S1) shows no material segregation, supporting the more homogenous material dispersion.

The composite materials (detailed compositions reported in Table 1) were tested in all-solid-state cells using LiI–Li_3PS_4 as solid electrolyte and Li metal as anode since this electrolyte shows a very stable interface with a metal electrode [30,31]. Galvanostatic cycling tests were performed with a specific current of 200 mA g^{-1} at 20 °C. Ex-situ XRD was used to study the reaction mechanism.

Fig. 2a, c shows the first discharge/charge voltage profiles of CuS and CuSC(3–2). The cell voltages at which ex-situ XRD patterns were acquired are also indicated. The most pronounced difference between the two cathodes can be appreciated in the first discharge profile. The carbon-free CuS shows two distinct plateaus at ca. 2.1 V and 1.4 V (Fig. 2a). This behavior is what we would normally expect from CuS, according to several previous studies that demonstrated a two-step mechanism [21,25,32,33]. The high voltage plateau is associated with the intermediate formation of cuprous sulfide (Cu_2S and other non-stoichiometric $Cu_{2-x}S$ phases, see reaction 2):

$$CuS + 1Li^+ + 1e^- \rightarrow ½\ Cu_2S + ½\ Li_2S \quad (2)$$

while at lower voltage metallic copper is extruded as result of Li diffusion in the Cu_2S structure:

$$Cu_2S + 2Li^+ + 2e^- \rightarrow 2Cu + Li_2S \quad (3)$$

The formation of metallic copper at the end of discharge (see reaction (3)) is clearly demonstrated by the very strong Cu^0 reflection evolving in the ex-situ XRD diffractogram (see Fig. 2b, related to the formation of micrometric copper dendrites. In fact, according to previous studies from Tarascon's and Adelhelm's groups [25,32], copper sulfides behave differently from sulfides of other metals such as Co and Ni. Specifically, during discharge, CuS does not form metallic Cu nano-particles embedded in a Li_2S matrix by conventional conversion. Instead, large Cu dendrites included in a Li_2S matrix are formed by a displacement reaction. However, based on our XRD results, no intermediate Cu_2S phase could be clearly detected upon the first reduction. This also applies to the activated carbon-containing CuSC(3–2) which, additionally, shows only a single plateau at 1.6 V (see Fig. 2c). Such behavior is normally expected

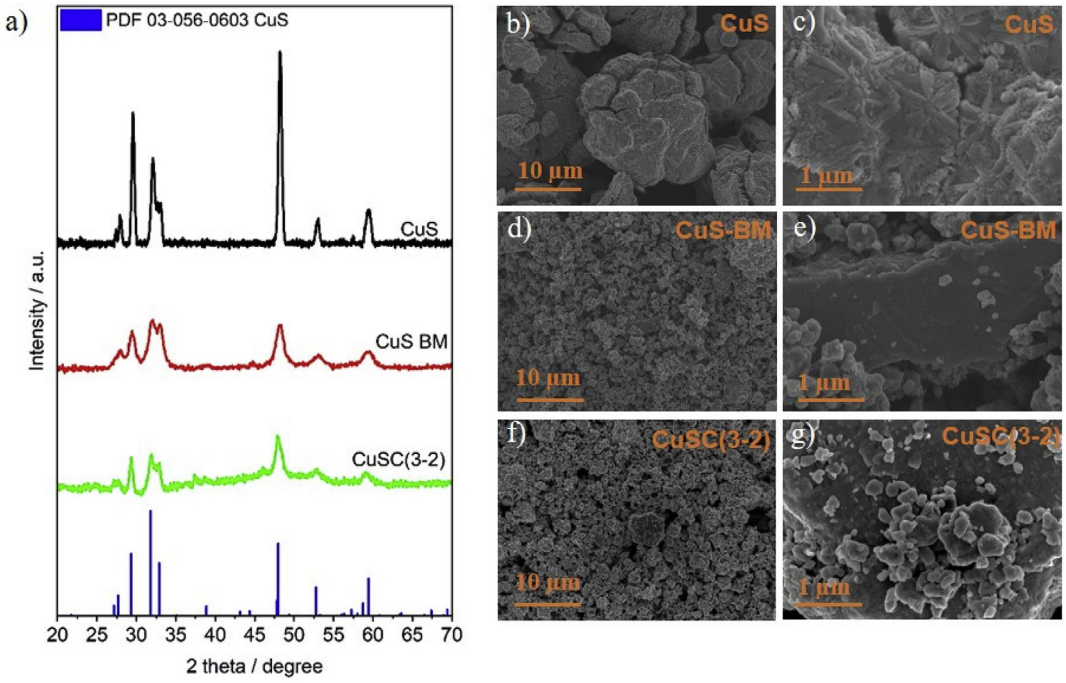

Fig. 1. a) XRD patterns of CuS as received, after ball milling (CuS-BM) and after incorporation in the CuSC(3–2) electrode. b-g) SEM images at different magnifications of the above mentioned materials (see caption in the panels). Note: no solid electrolyte is present in the samples.

Table 1
materials compositions and their respective theoretical capacities.

Name	CuS (wt %)	S (wt %)	C (wt %)	SE (wt %)	Theoretical capacity (mAh g^{-1})
CuS	50	–	–	50	560
CuSC(3–2)	30	–	20	50	560
CuSC(4–1)	40	–	10	50	560
CuSS(2–1)	20	10	20	50	910
CuSS(1-1)	15	15	20	50	1063
CuSS(1–2)	10	20	20	50	1286
SC(3–2)	–	30	20	50	1672

when starting from Cu_2S [32] but, again, no signatures from Cu_2S could be found either in the as-prepared powders (Fig. 1a) or the fresh cell (Fig. 2d). The previously mentioned reduction of crystalline size after ball milling with activated carbon could potentially explain this phenomenon. In fact, as shown by He et al. [34], non-equilibrium kinetic effects come into play when reducing the particle size to the nanoscale, causing a deviation from the thermodynamically expected two-step mechanism towards a single, flattened, low voltage plateau. It should be also noted that the low voltage plateaus of CuSC(3–2) and CuS are centered at 1.55 V and 1.4 V, respectively. This could be due to a lower polarization associated with the increased electronic conductivity of the CuSC(3–2) sample, as demonstrated by the EIS spectra of charged cells (see Fig S.2). For the CuSC(3–2) material at the end of the first discharge at 1.3 V (point b), the formation of metallic copper results in a five times decrease of the cell impedance compared to the charged state (see Fig S.3). However, there is no evident peak of crystalline Li_2S formation, indicating that Li_2S is amorphous or, alternatively, the crystallites are very small.

Another interesting point is that the pristine electrodes show additional diffraction peaks at 30.2°, 36.7°, and 45.4° 2θ degrees, potentially ascribable to copper phosphorus iodide sulfide (Cu_6PS_5I). This is known to be an argyrodite compound with high electronic and ionic conductivity, and suggest a reaction occurring between the solid electrolyte and copper sulfide [35,36]. This compound appears electrochemically active, since in the first discharge to 1.3 V its characteristic peaks vanish (see Fig. 2, point C for CuS and point b for CuSC(3–2)). Unfortunately, the peaks are rather small and the most intense one overlaps with those of CuS. Therefore, following the evolution of such a phase during cycling is very difficult. However, this side product certainly does not affect the Coulombic efficiency. In fact, as shown in Fig. 2e, the cathode composites containing Cu_6PS_5I (i.e., CuS and CuSC) show a remarkably high Coulombic efficiency of 99.9%, which is higher than a control electrode with S (i.e., 99.7% for SC(3–2), see Fig. 3c), which of course does not contain the side product. Upon the following charge, CuS display two clear plateaus at 1.8 V and 2.2 V associated with the reverse of reaction (3) and (2), respectively. Differently, the voltage profile of CuSC(3–2) lacks the feature at 2.2 V, while a larger capacity is observed for the low voltage plateau at 1.8 V. This suggests that the electrochemical mechanisms differ during charge too.

The cycling performance of the CuS and CuSC(3–2) materials in the solid-state cells is depicted in Fig. 2e. It can be clearly seen that the activated carbon has a key rule for ensuring good cycle life. Indeed, the addition of carbon can buffer the volume change upon de/lithiation and, therefore, improve the cycling stability [4]. As a matter of the fact, CuS shows a higher initial discharge capacity of about 590 mAh g^{-1}, which is very close to the theoretical value. This electrode material also shows an increase in capacity and a decrease in Coulombic efficiency upon the first 10 cycles. The increased capacity is due to the activity of the solid electrolyte and the formation of elemental sulfur, whereas, the decrease in Coulombic efficiency might be due to lack of carbon as a buffer for the volume change upon lithiation, therefore, affecting the reversibility of the redox reaction in the first few cycles. However, the following cycles, up to the 100th, reveal its continuous capacity fading, with a Coulombic efficiency of 99.8%. Instead, CuSC(3–2) shows lower initial discharge capacity, around 480 mAh g^{-1}, which, however, increases to 970 mAh g^{-1} over 800 cycles with a Coulombic efficiency of 99.9%. Selected voltage profiles of the cells including CuS and CuSC(3–2) electrodes are displayed in Fig. 2f, g, respectively. The discharge profiles of the CuS electrode maintains the two main plateaus, as previously discussed. Interestingly, after the second discharge the second plateau shifts to higher voltages (>1.6 V), probably due to the increased electronic conductivity caused by the formation of metallic copper.

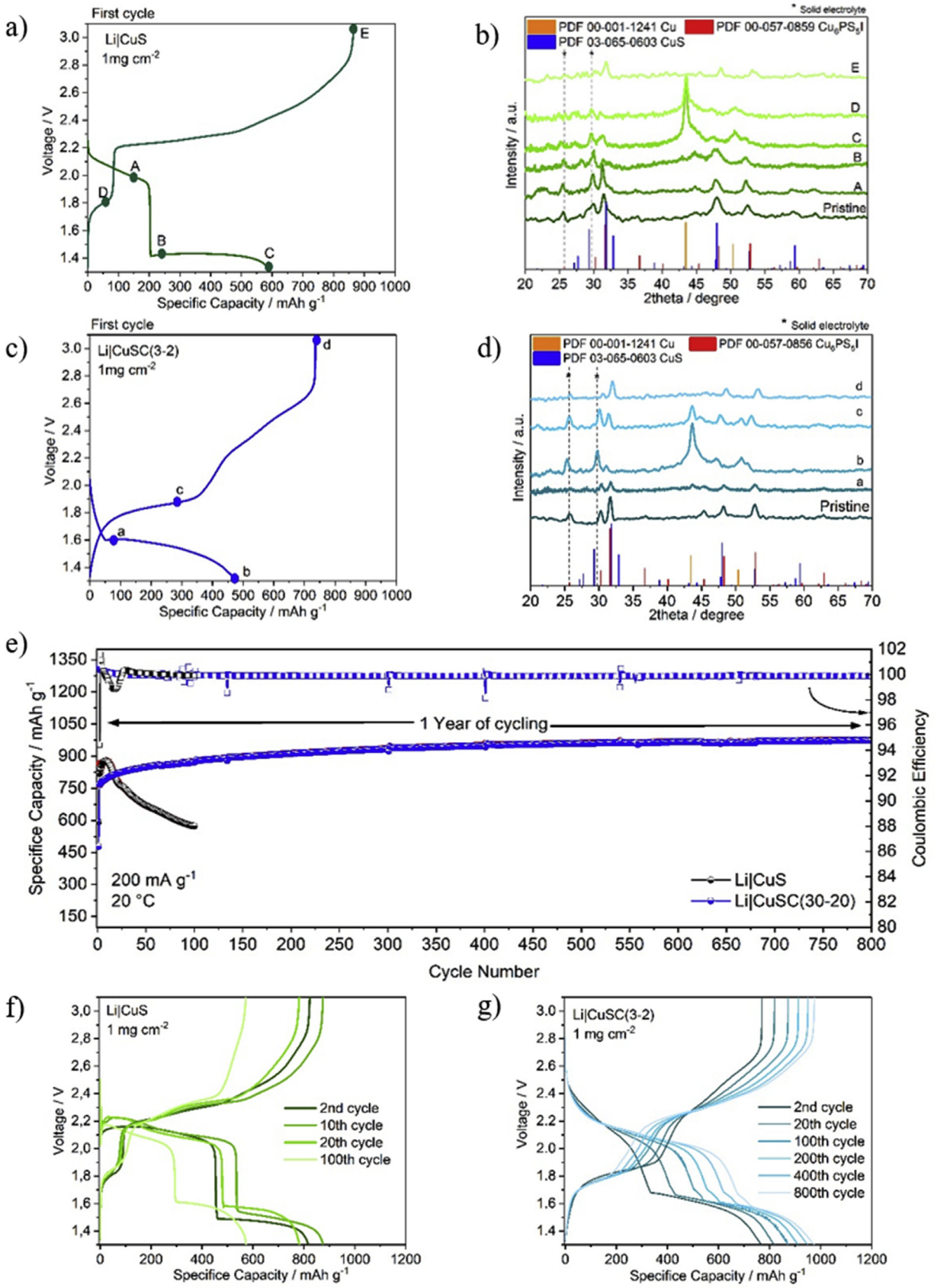

Fig. 2. First cycle voltage profiles and ex-situ XRD patterns (note: the two peaks around 25.6° and 29.7° (2θ) are characteristic of the solid electrolyte (see Fig S.4)) of a,b) CuS and c,d) CuSC(3–2) electrode materials. e) Capacity retention of CuS and CuSC(3–2) electrodes. Voltage profile evolution of f) CuS and g) CuSC(3–2) electrodes upon cycling. All measurements at 20 °C with 200 mA g^{-1} (0.177 mA cm^{-2}).

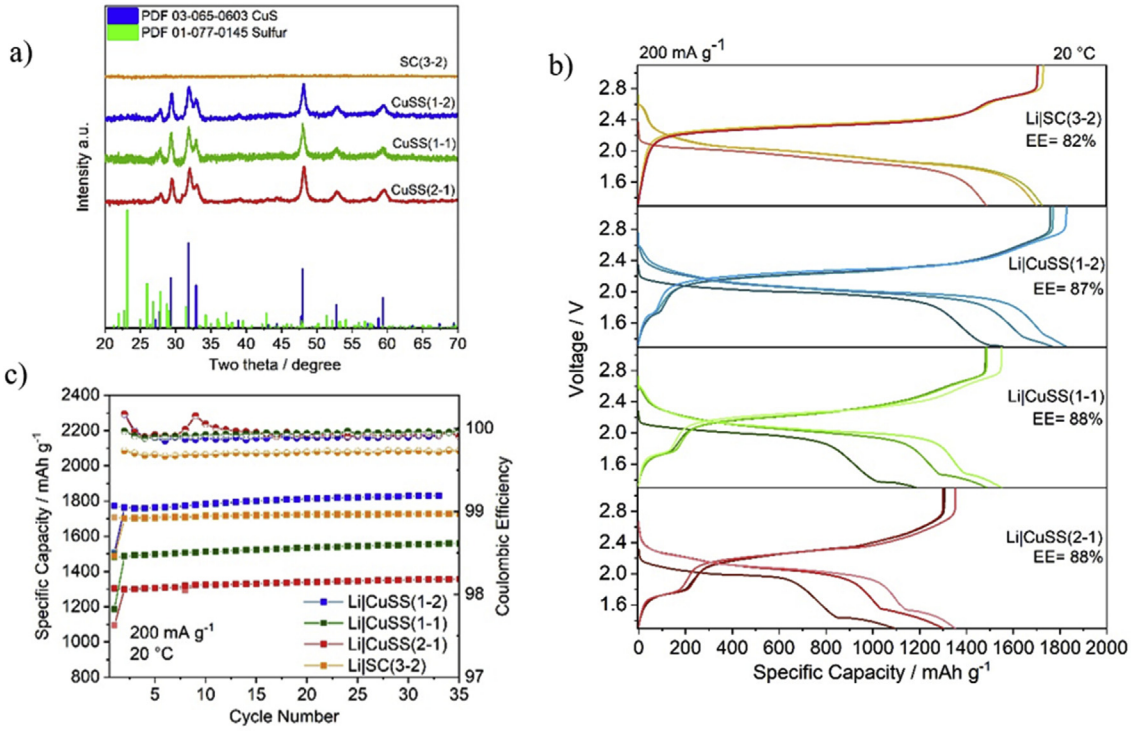

Fig. 3. a) XRD patterns of CuSS(2–1), CuSS(1-1), CuSS(1–2) and SC(3–2) pre-composite materials after the first ball milling step (i.e., prior to the addition of the solid electrolyte in the composites). Galvanostatic cycling test of the composite electrode materials (i.e., including the solid electrolyte): b) voltage profiles in the 1st, 2nd and 30th cycle and c) delivered capacity and Coulombic efficiency vs cycle number. All measurements at 20 °C with 200 mA g^{-1} (0.177 mA cm^{-2}).

In the charging step, the capacity delivered by the flat region at 1.8 V is 150 mAh g^{-1} lower than the corresponding reaction in discharge. It is also worth noticing that the capacity delivered at low potential is relatively constant, whereas the capacity at high potential decays over cycling.

Upon cycling, the discharge profile of the CuSC(3–2) electrode also evolves into two main plateaus centered at 2.1 V and 1.6 V similar to CuS. Interestingly though, the capacity delivered at the high voltage plateau increases over cycling (more than 250 mAh g^{-1}), while the low potential plateau is shortened (of about 200 mAh g^{-1}). This indicates that the reduction of copper sulfide to form Li_2S and Cu^0 may be partially irreversible. Very likely, the Cu^0 formed during discharge is not completely oxidized to CuS in the following charge, resulting in the formation of elemental S in the cathode. Therefore, on the following discharge step S is also active, providing a larger capacity at higher voltages. This may be the reason for the capacity retention of 130% after 800 cycles. It should be mentioned that, for both samples, the electrochemical activity of the solid electrolyte contributes to the capacity above 2.6 V, which is due to the redox reaction of LiI and Li_3PS_4, well documented already in the literature (see Fig S.5) [20,37]. The above-mentioned voltage profile evolution is better seen in the differential capacity plots (see Fig S.6). The intensity increase of the peak at 2.3 V may be attributed to the reactivity of sulfur. On the other hand, the low voltage peak intensity at 1.85 V decreases, which can again suggest the decreased contribution of CuS conversion to the overall capacity. A new peak around ca. 1.7 V during discharge also evolves upon cycling. The associated small plateau suggests the formation of new phases during extended cycling. The exact nature of these phases is still unknown and further measurements are required to fully disclose the reaction mechanism of this material in all-solid-state battery configuration.

To further investigate the differences introduced by the C in the CuSC composite, an additional electrode material characterized by a higher CuS/C ratio was also investigated (see Fig S.7), which, however, did not outperform CuSC(3–2) with 20 wt% carbon content. For such a reason CuSC(3–2) was selected for all further studies reported in this manuscript.

In order to further increase the specific capacity of the cathode, sulfur-copper sulfide-carbon (CuSS) composites, with varying rations have been prepared. Fig. 3a shows the XRD patterns of CuSS(2–1), CuSS(1-1), and CuSS(1–2) prior to the addition of the solid electrolyte (i.e., after the first ball milling step). The composite materials including the solid electrolytes (i.e., after the second ball milling step) show a more amorphous structure (Fig S.8). It can be seen that, in all samples, the pure CuS phase is retained (Covellite, ICDD PDF 03-065-0603, hexagonal, P63/mmc space group). No evidence of crystalline sulfur is observed, suggesting its complete amorphization during the milling process in the presence of carbon. In fact, crystalline sulfur can be detected in the diffractogram of the CuS and S binary mixture (Fig S.9). The addition of elemental sulfur in the composite electrodes seems also to hinder the formation of the Cu_6PS_5I phase observed before (Fig S.9). The soft sulfur may uniformly coat the CuS surface, thus decreasing the reactivity of the metal sulfide towards the solid electrolyte [20].

The composites were tested under galvanostatic conditions to evaluate their electrochemical behavior. Fig. 3b and c shows the voltage profile and cycling performance of all-solid-state Li metal anode cells, using LiI–Li_3PS_4 as the solid electrolyte and the CuSS composites as the positive electrode recorded at 20 °C and current density of 200 mA g^{-1}. The specific capacity is calculated on the total mass of copper sulfide and sulfur. All composites show specific capacities higher than the theoretical value (see data in Table 1) as the result of the well-known redox activity of the solid electrolyte between 2.6 and 2.8 V [20,37]. The voltage profiles of the three composite electrodes are very similar, consisting of two main plateaus (see Fig. 3b). The low voltage plateau around 1.6 V is due to the conversion of CuS while the high voltage region above 2.2 V arises from the S redox process. As expected, the capacity arising from these two distinct regions varies according to the electrode composition, with the low voltage plateau, i.e., the reduction of CuS to Cu^0 and Li_2S, shortening as the sulfur content is increased. Most importantly, however,

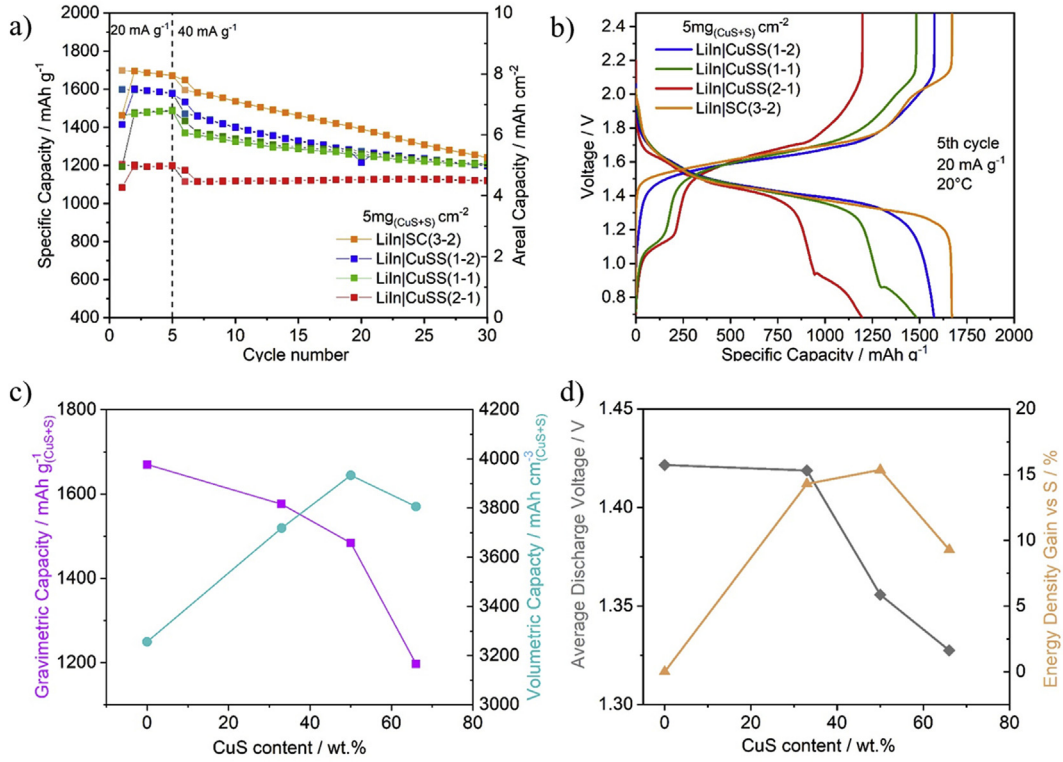

Fig. 4. a) Galvanostatic cycling and b) fifth cycle voltage profile of CuSS(2–1), CuSS(1-1), CuSS(1–2) and SC(3–2) composite electrodes with 5 $mg_{(CuS+S)}$ cm^{-2} areal loading. The first five cycles with 20 mA g^{-1} (0.085 mA cm^{-2}) and the rest of cycles with 40 mA g^{-1} (0.177 mA cm^{-2}) c) Gravimetric capacity and volumetric capacity versus CuS content, (d) Average discharge voltage and energy density gain versus CuS content.

the introduction of CuS in the composite electrodes substantially decreases the cell polarization. All cells employing the CuS-based cathodes show average voltages above 1.95 V and below 2.26 V during discharge and charge, respectively. On the contrary, the SC(3–2) control cell displays much larger polarization with average voltages of 1.93 V and 2.33 V. Such lower polarization naturally results in increased energy efficiency, up to 88% (see values in Table S.2). Furthermore, the CuSS(1–2) materials deliver higher capacity and high average discharge voltage than the SC(3–2), which results in a 5% increase of energy stored in the same mass of active material.

As shown in Fig. 3c, the CuSS(1–2) composites enable cycling stability comparable to the sulfur-carbon cathode but substantially improved Coulombic efficiency (above 99.8%) than SC(3–2) (99.6%). It is worth mentioning that the elongation of the high voltage plateau and the shortening of the low voltage plateau, which was previously observed for the CuSC(3–2) material (see Fig. 2g), is also evident in case of the CuSS materials. Whereas SC(3–2) does not show the increase in capacity, but rather starts to slightly decay after 25 cycles.

So far, the investigations have been performed on electrodes with a relatively low areal loading (1 mg cm^{-2} corresponding to 0.7–1.6 mAh cm^{-2}) to limit the mass transport effect and better understand the electrochemical reactions occurring in the various composites. However, in order to reach high energy density in practical batteries, higher active material areal loadings, i.e., 4–5 mg cm^{-2}, are required [38]. Fig. 4 shows the cycling performance of cells employing the previously studied electrode composites with a 5 $mg_{(CuS+S)}$ cm^{-2} loading. The measurements were performed at 20 °C using Li–In alloy negative electrodes in the all-solid-state configuration. This choice was not dictated by the instability of the solid electrolyte versus Li, which is in our case very good (as proven by the long cycling stability previously shown for areal loadings of 1 mg cm^{-2} (Fig. 2e) and 5 mg cm^{-2} (Fig. S.10)). Instead, LiIn was selected as an alloying anode to avoid cell failures associated with dendrite growth on Li, thus masking the intrinsic stability of the cathode.

The capacities delivered by the composite electrodes at 20 mA g^{-1} are 1600, 1450 and 1200 mAh g^{-1} for CuSS(1–2), CuSS(1-1) and CuSS(2–1), respectively. It is worth mentioning that the capacity decrease compared to the 1 mg cm^{-2} areal loading cells is remarkably low (between 150 and 50 mAh g^{-1}), even considered the lower current density. The highest areal capacity achieved in this work is 7 mAh cm^{-2} which clearly shows a better performance compare to recent publications (see values in Table S.1) [39]. The benefit of CuS compared to our previous work exploiting FeS_2–S composites is certainly related to the higher conductivity of both Cu^0 and CuS compared to Fe^0 and FeS_2. The formation of Cu^0 seems to be also an important factor in the stable cycling of the composite. In fact, the CuSS(2–1) material, although showing the low voltage plateau of CuS reduction, displays improved cycling stability compared to the CuSS(1–2) material, which lacks such a feature (see Fig. 4b). CuSS(1-1) also shows the low voltage plateau and stable response during the first five cycles, however, a capacity loss can still be appreciated in the longer term.

Overall, in order to achieve stable cycling at high loading, a price must be paid in terms of delivered capacity. In fact, the stable CuSS(2–1) delivers 470 mAh g^{-1} less than the control SC(3–2) cathode. It should be noticed, though, that CuS is more than twice as dense as S (4.76 g cm^{-3} and 2.07 g cm^{-3}, respectively) [40]. As a result, the volumetric capacity of all CuS–S mixtures is always higher than pure S (see Fig. 4c, and Table S.3 for details). Interestingly, this even compensates for the lower average discharge voltage caused by the CuS conversion, leading to potential energy density gains from 9 to 15% (see Fig. 4d).

3. Conclusions

Copper sulfide-sulfur composite electrodes were successfully prepared by simple and relatively cheap mechanochemical procedure and implemented in all-solid-state cells using LiI–Li_3PS_4 as the solid electrolyte. The solid electrolyte and copper sulfide appear to react together

upon ball milling to prepare the composite electrode powder, producing Cu_6PS_5I. However, such a reaction is hindered by the presence of sulfur, as evidenced by XRD.

The carbon/CuS ratio plays a crucial role in achieving stable cycling, as well as determining the reaction mechanism of the copper sulfide cathode, especially upon the first reduction. The Li|CuSC(3–2) cell with mass loading of 1 $mg_{(CuS)}$ cm^{-2}, delivers a specific capacity above 850 mAh g^{-1} for more than 800 cycles at 20 °C. The reduction of copper sulfide to metallic copper upon discharge was confirmed by XRD. Copper sulfide-sulfur composite electrodes with mass loading of 1 $mg_{(CuS+S)}$ cm^{-2} deliver high specific capacities above 1790 mAh g^{-1} at 20 °C using Li^0 as the negative electrode. High areal capacities, up to 7 mAh cm^{-2}, were achieved at 20 °C with the CuSS(1–2) composite electrode using a mass loading of 5 $mg_{(CuS+S)}$ cm^{-2} and a LiIn anode. The incorporation of copper sulfide in composite sulfur cathodes also improves cyclability and energy efficiency (by decreasing the cell polarization). Finally, it should be noted that the higher density of CuS compared to S leads to an increased volumetric capacity and, potentially, higher energy density. The best trade-off may be found with the CuS-rich cathode CuSS (2–1), delivering stable cycling performance at high loading (1200 mAh cm^{-2} and 1100 mAh cm^{-2} at 20 and 40 mA g^{-1}, respectively) and ca. 9% potential energy density gain with respect to a conventional Carbon–Sulfur cathode. The calculation is solely done with the purpose of estimating the potential energy density gain with respect to the control cathode composition SC (3–2). We are aware that many parameters need to be optimized in order to employ these composite cathodes in practical cells. In particular, carbon and solid electrolyte content must be substantially decreased. Preliminary data show that the carbon content can be substantially decreased without dramatically affecting the performance. On the other hand, reducing the solid electrolyte ratio requires some additional efforts, which will be the subject of our future work.

4. Experimental

4.1. Materials preparation

MAXSORB activated carbon (KANSAI COKE AND CHEMICALS CO., LTD.), elemental sulfur (99.998%, Sigma-Aldrich) and CuS (99.98%, Alfa-Aesar) were dried and transferred in an Ar-filled UNIlab glove box (MBRAUN, O_2 and H_2O < 0.1 ppm). LiI–Li_3PS_4 Solid electrolyte was received from SRJ japan and was prepared base on the previously reported mechanochemical synthesis [37]. Several composite materials, which composition is given in Table 1, were produced via ball-milling. The materials were weighted in the desired ratio and ground in an agate mortar. Each mixture was then transferred in a 45 mL ZrO_2 jar filled with ZrO_2 balls (10 g of 1 mm balls, seventeen 5 mm balls and ten 1 cm balls), which was sealed under inert Ar atmosphere using parafilm and an additional clamping system to avoid exposure to air. Finally, the composite materials were ball-milled in a Pulverisette 4 (FRITSCH), alternating a ball-milling step at 360 rpm (45 min) with a rest (cooling) step (15 min). This procedure was repeated for 17 times (total ball-milling time of ca. 13 h). The jars were then transferred in an Ar-filled glove box, the mixtures recovered and separated from the ZrO_2 balls, ground in an agate mortar and mixed in a 1:1 wt ratio with the Li_3PS_4–LiI (SE) solid electrolyte. The CuS-Sulfur-C/SE mixtures were then transferred in a 45 mL ZrO_2 jar filled with ZrO_2 balls (10 g of 1 mm balls, seventeen 5 mm balls and ten 10 mm balls), which was sealed under inert Ar atmosphere using parafilm and an additional clamping system to avoid exposure to air. Finally, the mixtures were ball-milled in a Pulverisette 4 (FRITSCH), alternating a ball-milling step at 360 rpm (45 min) with a rest (cooling) step (15 min) and repeated 17 times, to obtain the various composite electrode materials. These latter materials were recovered from the jar inside the argon-filled glove box and ground in an agate mortar prior to use for the electrochemical characterization. The composites component rations are confirmed with thermogravimetric analysis (TGA) see Fig. S.11.

4.2. Assembly of solid state cells

For cell assembly, an in-house, two-electrode (Ø = 13 mm) cell (Torque cell) was employed [41,42]. In detail, a cylindrical plastic case with an internal diameter of 13 mm was used as die-set for pellet preparation. For the low mass loading cells, lithium metal disks (thickness = 30 μm, Ø1.2 cm. Honjo Metal, Osaka) were used as a negative electrode. In fact, as proven by previous literature reports, the solid electrolyte used in this study forms a stable interface with Li metal [30,31]. For the high mass loading cells, the negative electrodes were composed of an indium metal disk (thickness = 100 μm, Ø1.2 cm. Sigma-Aldrich) hand pressed on top of a lithium metal disk. About 200–250 mg of LiI–Li_3PS_4 were introduced inside the die-set on top of the negative electrode disk and pressed by a hydraulic press (YLJ-24, MTI corp.) at 2 MPa to form a pre-pellet with thickness in the range of 650–850 μm. Afterward, a selected amount of the composite cathode material was spread over the electrolyte pre-pellet. The pre-formed cell was finally pressed at 10 MPa for 1 min, at 20 °C, using the hydraulic press. The cell was hosted in a metal case equipped with a screw applying force on the upper current collector and, therefore, ensuring the mechanical stability of the pelletized cell, as well as helping keep an intimate contact between the materials. The active material loading, considered as the total amount of CuS + S for the specific capacity calculation, ranged between 1.0 and 5.0 mg cm^{-2}. To carry out the electrochemical tests, the cells were additionally sealed in aluminum bags filled with Ar to avoid air contamination.

4.3. Electrochemical measurements

Galvanostatic cycling tests were performed in the 1.3–3.1 V and 0.68–2.48 V voltage range for Li and LiIn anode respectively, using a Maccor 4000 Battery Test System in thermostatic climatic chambers set at 20 °C, with a maximum deviation of ±1 °C. The cells were left to rest at open-circuit voltage conditions (OCV) for 24 h prior to testing. Electrochemical impedance spectroscopy was performed by means of a Solartron SI 1260 impedance/gain phase analyzer. EIS was measured from 1 MHz to 0.1 Hz at an AC amplitude of 10 mV.

4.4. Characterization

The morphological and structural characterization of all materials was performed by field emission scanning electron microscopy (SEM, Zeiss LEO1550VP Gemini) and X-ray diffraction (XRD Bruker D8 Advance diffractometer equipped with a CuK_α source $\lambda = 0.154$ nm). An airtight, Ar filled sample holder was used to transferring the samples from the glove box to the SEM chamber. For the XRD measurements, airtight sample holders were employed to avoid sample degradation. Thermo-gravimetric analysis (TGA) was performed under N_2 stream in a temperature range of 30–600 °C, with a constant heating rate of 10 °C/min by using a Discovery TGA (TA Instruments). To prevent contamination, the samples were sealed in aluminum airtight pans inside the glove box, which were open by the instrument immediately before the test.

Data statement

Due to the sensitive nature of the questions asked in this study, survey respondents were assured raw data would remain confidential and would not be shared.

Data not available/The data that has been used is confidential.

CRediT authorship contribution statement

Seyed Milad Hosseini: Investigation, Data curation, Writing - original draft. **Alberto Varzi:** Conceptualization, Validation, Writing - review & editing. **Seitaro Ito:** Investigation, Data curation, Writing - original

draft. **Yuichi Aihara:** Conceptualization, Validation, Writing - review & editing. **Stefano Passerini:** Conceptualization, Validation, Writing - review & editing.

Appendix A. Supplementary data

Supplementary data to this article can be found online at https://doi.org/10.1016/j.ensm.2020.01.022.

References

[1] N. Kamaya, K. Homma, Y. Yamakawa, M. Hirayama, R. Kanno, M. Yonemura, T. Kamiyama, Y. Kato, S. Hama, K. Kawamoto, A. Mitsui, Nat. Mater. 10 (2011) 682.
[2] J.C. Bachman, S. Muy, A. Grimaud, H.-H. Chang, N. Pour, S.F. Lux, O. Paschos, F. Maglia, S. Lupart, P. Lamp, L. Giordano, Y. Shao-Horn, Chem. Rev. 116 (2016) 140–162.
[3] A. Manthiram, Y. Fu, Y.-S. Su, Acc. Chem. Res. 46 (2013) 1125–1134.
[4] D.-W. Wang, Q. Zeng, G. Zhou, L. Yin, F. Li, H.-M. Cheng, I.R. Gentle, G.Q.M. Lu, J. Mater. Chem. 1 (2013) 9382–9394.
[5] P. Albertus, S. Babinec, S. Litzelman, A. Newman, Nature Energy 3 (2018) 16–21.
[6] X. Liu, J.-Q. Huang, Q. Zhang, L. Mai, Adv. Mater. 29 (2017), 1601759.
[7] X. Rui, H. Tan, Q. Yan, Nanoscale 6 (2014) 9889–9924.
[8] T. Takeuchi, H. Sakaebe, H. Kageyama, T. Sakai, K. Tatsumi, J. Electrochem. Soc. 155 (2008) A679–A684.
[9] W. Shi, J. Zhu, X. Rui, X. Cao, C. Chen, H. Zhang, H.H. Hng, Q. Yan, ACS Appl. Mater. Interfaces 4 (2012) 2999–3006.
[10] K. Chang, Z. Wang, G. Huang, H. Li, W. Chen, J.Y. Lee, J. Power Sources 201 (2012) 259–266.
[11] T. Matsumura, K. Nakano, R. Kanno, A. Hirano, N. Imanishi, Y. Takeda, J. Power Sources 174 (2007) 632–636.
[12] K. Tibbetts, C.R. Miranda, Y.S. Meng, G. Ceder, Chem. Mater. 19 (2007) 5302–5308.
[13] C. Xu, Y. Zeng, X. Rui, N. Xiao, J. Zhu, W. Zhang, J. Chen, W. Liu, H. Tan, H.H. Hng, Q. Yan, ACS Nano 6 (2012) 4713–4721.
[14] X. Yao, D. Liu, C. Wang, P. Long, G. Peng, Y.-S. Hu, H. Li, L. Chen, X. Xu, Nano Lett. 16 (2016) 7148–7154.
[15] I. Belenkaya, S. Menkin, H. Mazor, T. Mukra, L. Burstein, Y. Rosenberg, A. Gladkich, D. Golodnitsky, J. Solid State Electrochem. 23 (419) (2019).
[16] V. Pelé, F. Flamary, L. Bourgeois, B. Pecquenard, F. Le Cras, Electrochem. Commun. 51 (2015) 81–84.
[17] E. Strauss, D. Golodnitsky, E. Peled, Electrochim. Acta 45 (2000) 1519–1525.
[18] E. Kendrick, J. Barker, J. Bao, A. Świątek, J. Power Sources 196 (2011) 6929–6933.
[19] J. Barker, E. Kendrick, J. Power Sources 196 (2011) 6960–6963.
[20] U. Ulissi, I. Seitaro, H.S. Milad, V. Alberto, A. Yuichi, P. Stefano, Advanced Energy Materials, 2018, 1801462.
[21] J.S. Chung, H.J. Sohn, J. Power Sources 108 (2002) 226–231.
[22] J. Balach, J. Linnemann, T. Jaumann, L. Giebeler, J. Mater. Chem. 6 (2018) 23127–23168.
[23] I. Exnar, J. Hep, J. Power Sources 44 (1993) 701–705.
[24] J.P. Gabano, V. Déchenaux, G. Gerbier, J. Jammet, J. Electrochem. Soc. 119 (1972) 459–461.
[25] A. Débart, L. Dupont, R. Patrice, J.M. Tarascon, Solid State Sci. 8 (2006) 640–651.
[26] K. Sun, C. Zhao, C.-H. Lin, E. Stavitski, G.J. Williams, J. Bai, E. Dooryhee, K. Attenkofer, J. Thieme, Y.-c.K. Chen-Wiegart, H. Gan, Sci. Rep. 7 (2017), 12976.
[27] N. Machida, K. Kobayashi, Y. Nishikawa, T. Shigematsu, Solid State Ionics 175 (2004) 247–250.
[28] A. Hayashi, T. Ohtomo, F. Mizuno, K. Tadanaga, M. Tatsumisago, Electrochem. Commun. 5 (2003) 701–705.
[29] M. Pentimalli, M. Bellusci, F. Padella, High-energy ball milling as a general tool for nanomaterials synthesis and processing, in: M. Aliofkhazraei (Ed.) Handbook of Mechanical Nanostructuring 2015.
[30] F. Han, J. Yue, X. Zhu, C. Wang, Advanced Energy Materials 8 (2018) 1703644.
[31] M. Suyama, A. Kato, A. Sakuda, A. Hayashi, M. Tatsumisago, Electrochim. Acta 286 (2018) 158–162.
[32] B. Jache, B. Mogwitz, F. Klein, P. Adelhelm, J. Power Sources 247 (2014) 703–711.
[33] K. Jiang, Z. Chen, X. Meng, ChemElectroChem 6 (2019) 2825–2840.
[34] K. He, Z. Yao, S. Hwang, N. Li, K. Sun, H. Gan, Y. Du, H. Zhang, C. Wolverton, D. Su, Nano Lett. 17 (2017) 5726–5733.
[35] R.B. Beeken, J.J. Garbe, N.R. Petersen, J. Phys. Chem. Solid. 64 (2003) 1261–1264.
[36] A. Gągor, A. Pietraszko, D. Kaynts, J. Solid State Chem. 178 (2005) 3366–3375.
[37] Y. Aihara, S. Ito, R. Omoda, T. Yamada, S. Fujiki, T. Watanabe, Y. Park, S. Doo, Frontiers in Energy Research 4 (2016).
[38] H.-J. Peng, J.-Q. Huang, X.-B. Cheng, Q. Zhang, Advanced Energy Materials 7 (2017), 1700260.
[39] R. Xu, J. Yue, S. Liu, J. Tu, F. Han, P. Liu, C. Wang, ACS Energy Letters 4 (2019) 1073–1079.
[40] W.M. Haynes, D.R. Lide, T.J. Bruno, C.R.C. Press, CRC Handbook of Chemistry and Physics : a Ready-Reference Book of Chemical and Physical Data, 2013.
[41] S. Ito, S. Fujiki, T. Yamada, Y. Aihara, Y. Park, T.Y. Kim, S.-W. Baek, J.-M. Lee, S. Doo, N. Machida, J. Power Sources 248 (2014) 943–950.
[42] U. Ulissi, M. Agostini, S. Ito, Y. Aihara, J. Hassoun, Solid State Ionics 296 (2016) 13–17.